Taylor & Francis
Taylor & Francis Group

Drying Technology
An International Journal

ISSN: 0737-3937 (Print) 1532-2300 (Online) Journal homepage: www.tandfonline.com/journals/ldrt20

Exploring agglomeration: The role of particle size and shape in binary collisions

S. W. C. de Leeuw, N. M. Eijkelboom, K. Hoonings, A. López Rochés, R. G. M. van der Sman & M. A. I. Schutyser

To cite this article: S. W. C. de Leeuw, N. M. Eijkelboom, K. Hoonings, A. López Rochés, R. G. M. van der Sman & M. A. I. Schutyser (24 Dec 2025): Exploring agglomeration: The role of particle size and shape in binary collisions, Drying Technology, DOI: 10.1080/07373937.2025.2606964

To link to this article: https://doi.org/10.1080/07373937.2025.2606964

Published online: 24 Dec 2025.

DRYING TECHNOLOGY
https://doi.org/10.1080/07373937.2025.2606964

Exploring agglomeration: The role of particle size and shape in binary collisions

S. W. C. de Leeuw[a], N. M. Eijkelboom[a], K. Hoonings[a], A. López Rochés[a], R. G. M. van der Sman[b], and M. A. I. Schutyser[a]

[a]Laboratory of Food Process Engineering, Wageningen University & Research, Wageningen, the Netherlands; [b]Food and Biobased Research, Wageningen University & Research, Wageningen, the Netherlands

ABSTRACT

In spray drying operations, fines are recovered and recirculated into the dryer to enhance agglomeration. Since the properties of fines may affect collision outcomes, this study aims to specifically investigate the impact of varying particle size and shape on collisions. Given the challenging conditions of a spray dryer, a custom-built single droplet dryer was used to study collision behavior. This allowed for dispensing and drying of a sessile droplet and controlled collisions of small fines particles using the air flow. First, glass beads with different size ranges were employed to collide with drying maltodextrin droplets. Sequential merging, sticking and bouncing regimes were observed, where the regimes were affected by fine particle size. A larger particle size led to more sticking and fewer bouncing collisions. Additional experiments were carried out with maltodextrin particles which have a lower density and a non-spherical shape. Minor differences were found if maltodextrin particles and glass beads were compared. Mostly, it was observed that drying time and thus the state of the droplet skin is dominant in determining the collision outcome. Obtained insights are useful to establish future guidelines for nozzle zone agglomeration in spray drying

ARTICLE HISTORY
Received 19 September 2025
Revised 2 December 2025
Accepted 15 December 2025

KEYWORDS
Single droplet drying; agglomeration; collision outcome; particle size; particle shape

Introduction

Spray drying is one of the most common drying techniques in the food industry, typically for dairy powder formulations, yeast, flavor ingredients, and also plant-based alternatives. Spray drying is widely used since it is a mild drying technique, it is well scalable and it provides high quality and functional powders. The spray drying process involves atomization of a solution into very small droplets, after which droplets are exposed to hot, dry air. This process allows for fast evaporation at relatively low temperatures. Dry particles are collected and separated from the outgoing air. Very small particles ($<100\,\mu m$), called fines, are usually recirculated into the spray dryer to enhance nozzle zone agglomeration.[1] Agglomeration improves the techno-functional properties of spray dried powders, such as flowability and reconstitution behavior, desired for high quality food powders.[2] However, controlling agglomeration during spray drying is currently still based on empirical guidelines, while it is critical to guide product quality and prevent production of off-spec powders.

Agglomeration mostly occurs in the nozzle zone, where partially dried droplets can form agglomerates upon collision, also with recirculated fines particles.[3] During droplet-droplet and droplet-particle collisions different regimes are distinguished. If a droplet still has liquid-like properties, collisions with dry particles lead to penetration of the dry particles into the droplet.[4] This is classified as a merging collision and usually occurs when the droplet temperature is still well above the glass transition temperature (T_g). When a smaller wet droplet collides with a larger solid particle, it might spread across the surface, which results in a coating effect. A bouncing collision outcome is observed when the skin of the drying droplet is dry and rigid and has reached its glassy state and the colliding particle or droplet is glassy as well.[5] For agglomeration it is most desired that the collision results in a dry particle, or semi-dried droplet,

CONTACT M. A. I. Schutyser maarten.schutyser@wur.nl Laboratory of Food Process Engineering, Wageningen University & Research, P.O. Box 17 6700 AA Wageningen, the Netherlands.

adhering to the surface of another semi-dried droplet. Sticking collisions usually occur close to the stickiness temperature, i.e. T_g+30 °C.[4,6,7] These sticking collisions are desired as larger porous agglomerates are formed, which benefit powder properties.

Throughout the drying process, droplets undergo significant physicochemical changes. During the first stage, mass and heat transfer are externally limited and so evaporation occurs rapidly, the so-called constant rate period. Upon further drying, a skin develops and reaches a strength that inhibits further isotropic shrinkage of the droplet. This point is referred to as the locking point.[8,9] At around the locking point time, evaporation becomes diffusion limited and morphology development commences. The properties of the droplet skin determine whether the skin can withstand developed stresses, and so what morphology is formed. For example, droplets consisting of smaller sugars do not develop a rubbery skin for some amount of time during drying, only viscous behavior was observed.[10,11] This skin cannot withstand the stresses exerted on the droplet surface and surface wrinkling is the result. This is different for larger sugars, where the rubbery skin causes cavitation.

Monitoring droplet drying and collision behavior is essential for understanding agglomeration and for better control of powder properties, yet this is challenging for large-scale spray drying. To overcome this challenge, single droplet drying (SDD) techniques have been employed to study droplet drying and agglomeration behavior from a more mechanistic perspective.[12] Specifically, in this study sessile single droplet drying was used. This method is straightforward if compared to other methods, since it allows for monitoring of droplet shrinkage, temperature and morphology development over time.[13,14] An inherent limitation of this approach is the effect of the surface, resulting in conductive heat transfer and so also contributing to evaporation. Using SDD approaches, for example, the impact of drying on bacterial survival, enzyme activity, particle morphology and solubility have been unraveled for a number of food and pharmaceutical matrices.[13–19]

Recently, a study utilized a sessile single droplet drying approach for studying binary collisions between drying droplets and glass beads, acting as fines particles.[20,21] It was shown that for collisions between maltodextrin droplets and glass beads, the stickiness regime ranges from approximately 0.75 to 1.5 times the normalized collision time ($t_{collision}/t_{lock}$). Additionally, it was shown that the formulation of the system, i.e. type of maltodextrin and/or presence of protein affected the stickiness regime and thus the outcome of the collisions. For these results, the binary collisions were performed using model glass bead fines of a specific size, whereas during spray drying fines particles have varying size, which can be expected to influence collision outcomes. Also, glass beads are spherical and have a significantly higher density, if compared to fines particles in industrial drying processes, which have an irregular shape and usually a lower density.

Therefore, the aim of this study is to investigate the effect of particle size and shape on the binary collisions of particles and drying droplets. Next to glass beads of varying size, also maltodextrin particles were used as more realistic fines material. A custom-built sessile single droplet dryer was operated, where a particle dosing system was used to perform controlled collision studies. Collisions were monitored using a high-speed camera and further evaluated *via* image analysis.

Materials & methods

Materials

Maltodextrin (MD) is chosen as the model component for making the droplet solutions. MD is a well-defined polymer with well characterized physical properties (e.g. diffusivities, sorption isotherms) and so ideal for physical modeling. This choice is thus of interest for understanding the phenomena of agglomeration. The dried droplets consisted of a solution of maltodextrin with dextrose equivalent (DE) of 38 (Glucidex 38, Roquette Frères, Lestrem, France). The major focus in this study is on the effect of particle collision materials. For collision experiments glass beads were obtained from EPCE bouwstoffen B.V. (the Netherlands), in the size ranges 0–50, 70–110, 90–150 and 150–250 µm (density of 3220 kg/m^3). The other collision material used was maltodextrin powder with a dextrose equivalent of 21 (Glucidex 21, Roquette Frères, Lestrem, France). Maltodextrin powder was mixed with the silica-based flow aid Sipernat 380 (manufactured by Evonik Industries, supplied by Azelis, Merelbeke, Belgium).

Sample preparation

Maltodextrins DE38 solutions of 20% (w/w) were prepared with demineralized water. The mixtures were stirred for 30 min at 300 rpm to obtain transparent, homogeneous solutions. Maltodextrin DE21 used as collision material was separated using an Airjet Sieve

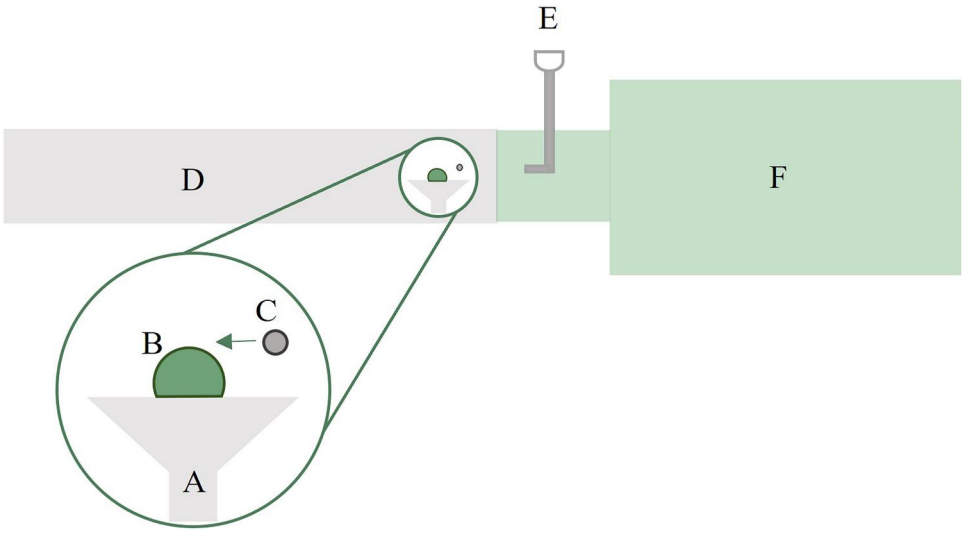

Figure 1. Schematic overview of sessile single droplet drying platform, extended with collisions, adapted from Eijkelboom et al.[21] A: Drying table, B: Droplet on table, C: Dry particle trajectory, D: Drying chamber, E: Dry particle reservoir with tube attached, F: Heating block for heating drying air.

E200 LS (Hosokawa Alpine, Augsburg, Germany) and a sieve pore size of 200 µm. For the next step, only the fraction with a particle size greater than 200 µm was used, given small powder particles decrease powder flowability. Flow aid Sipernat 380 (4% w/w) was added to 10 g maltodextrin powder using a farinograph (Torque Rheometer Processor with DO-Corder E330 drive unit, Brabender GmbH & Co. KG, Duisberg, Germany). The powder was mixed for 45 min at 50 rpm. Addition of the flow aid was done to enhance flowability and successfully disperse the MD powder in the SDD system. The final particle size distribution of prepared MD powder ranged from approximately 10 to 350 µm (Appendix, Figure A2).

Sessile single droplet drying extended with collisions

A custom-built sessile single droplet dryer was used for dispensing and drying droplets on a surface. An overview of the setup can be found in Figure 1. Droplets of with a diameter of 400 µm were dispensed on the drying table. Droplet size used is at the upper limit, if compared to droplets atomized in a spray dryer, which are usually around 30–250 µm.[22] Larger droplets were selected for slower drying, ensuring more accurate information about the stickiness regime. Very fast initial drying makes it challenging to observe sticking collisions and more accurate monitoring of the transition from merging to sticking and bouncing provides better mechanistic understanding of binary collisions between a dry particle and a drying droplet. Drying was performed using representative outlet air conditions of 80 °C at 0.4 m/s, which is common practice in sessile droplet drying studies.[8] Also, droplets mostly experience outgoing air conditions during spray drying. Given the focus of this research is on the use of collision materials, the sample preparation and drying of the droplet was kept constant throughout the experiments.

To carry out collision experiments, the sessile single droplet drying platform was extended. To enforce collisions, first approximately 25 mg of dry particles were loaded into the dry particle reservoir. When triggered the reservoir would flip over, dropping the dry particles into a small tube. At the bottom of the tube the dry particles were dragged along with the air stream to finally reach the dispensed drying droplet. A specific time for switching the reservoir, and so for collisions, was put in the system, varying from 1 to 12 s for both glass beads and MD particles. At least 10 collision measurements were captured per time point for every particle size/type. For an extensive description of the experimental setup and the procedure used for experiments, the reader is referred to Eijkelboom et al.[20]

Collision particle characterization

Size characterization was carried out for both the maltodextrin powder and the glass beads. A Mastersizer 3000 (Malvern Panalytical, UK) was used to observe the particle size distribution (PSD_Mastersizer) (Appendix, Figure A1).

To obtain the variation in particle shape and size, the specific area and circularity of the colliding

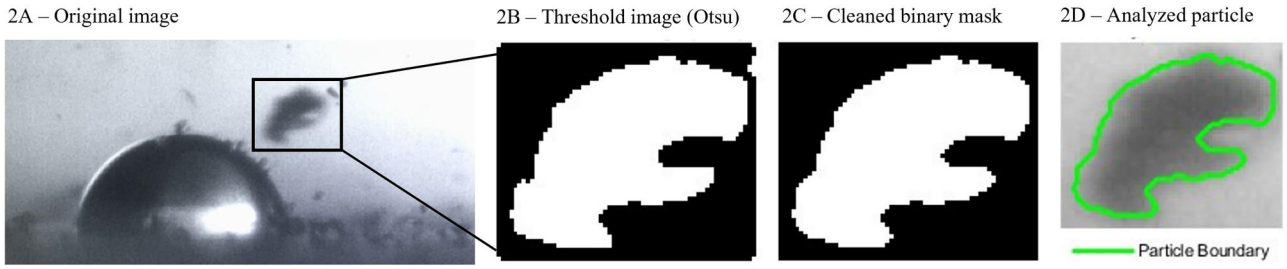

Figure 2. Overview of selection and analysis of dry particle: (A) original image, (B) mask obtained through Otsu thresholding, (C) cleaned mask, (D) visualization of analysis of perimeter of dry particle.

particles was analyzed from the movies using MATLAB (MathWorks, USA). First, Contrast Limited Adaptive Histogram Equalization (CLAHE) was used to enhance the local contrast in the image and the frame was smoothed to preserve the edge of objects. This method is commonly used to improve image quality and detection accuracy, especially in images with very dark or bright regions. This method is for example applied in ocean engineering and diagnosing retinal diseases.[23,24] Next, Otsu's method was used to determine a threshold that separates foreground from background by creating a mask (Figure 2(B)). This method has been applied for example to separate text from the background in an image and for image analysis of gel electrophoresis.[25,26]

The created mask was smoothed using morphological operators (Figure 2(C)). Next, the perimeter and circularity were determined (Figure 2(D)). For the perimeter the function regionprops was used, which uses subpixel resolution by default for a more accurate estimation of the perimeter.[27] The sum of the length of the edges around the object was calculated and no shape assumptions were made. Subsequently, the particle area was calculated by determining all pixels within the detected edges.

Single droplet drying and collision analysis

Movie analysis

The locking point time (t_{lock}) and collision outcome were visually observed from the movies and the exact time of collision ($t_{collision}$) was extracted. The collision outcomes were classified as merging, sticking or bouncing. The collision outcome was marked as merging when there was complete submerging of the dry particle into the droplet. The collision outcome was marked as sticking when the dry particle adhered to the surface, this could also mean partly submerging of the particle with the droplet. The collision outcome was classified as bouncing when, after colliding, the particle distinctly rebounded from the droplet. Probability plots were generated based on kernel density estimation, as explained in Eijkelboom et al.[20]

Additionally, the image analysis toolbox from MATLAB (MathWorks, USA) was used to determine the droplet diameter over time, up until the locking point. A spherical cap was constructed and the subsequent volume was determined using pixel count. From this the droplet diameter was determined over time, up until the locking point. The average linear decrease can be found in the Appendix, Figure A3. Next, using the image analysis toolbox again from MATLAB (MathWorks, USA) the diameter of each glass particle colliding with the drying droplet was determined. The output of the analysis included a visual check for correctly identifying the colliding particle, as visualized in Figure 3. A complete PSD was obtained (PSD_Matlab), which can be found in Appendix, Figure A2.

Data processing

All obtained collision data was plotted as the normalized particle diameter (d_p/d_d) over the normalized collision time ($t_{collision}/t_{lock}$) (Appendix, Figure A4), with d_p the diameter of the dry glass bead and d_d the droplet diameter, which decreases over time. Given that evaporation becomes diffusion-limited during the falling rate period, evaporation slows down significantly after the locking point. For that reason, it was assumed the droplet remains at a constant volume after the locking point, for a drying time up until 12 s.

Subsequently, a 2D grid of 100×100 evenly spaced points was constructed across the spatial extent defined by the scatter plot. For each grid point a circular neighborhood of radius $r = 0.1$ was defined to identify all nearby data points. If the number of neighboring samples was ≥ 3 the relative frequency of each outcome was computed and stored as local probability estimate. For the interpolation a Radial Basis function (RBF) with a multiquadric kernel was used. The smoothing parameter was set to 0.05, to generate smooth probability fields. RBF's are applied for

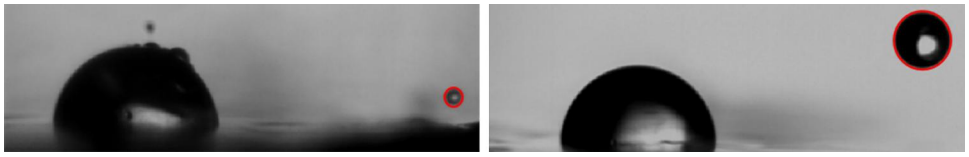

Figure 3. Output from the MATLAB anaylysis, for visual check of selected glass bead. The red circle marks the detected particle. From the particle selection the radius was calculated in the script.

approximating multivariable functions using the distance between the input and a fixed point. They are often used for forecasting, such as for estimating volume fractions of oil–gas–water mixtures in a pipeline in the petroleum industry and predicting flood water levels.[28,29] The interpolated maps were stacked to identify the most probable outcome at each grid point using argmax. Classification certainty was estimated as the difference between the top two probabilities, where a small difference between those was classified as highly uncertain. The classification was smoothed using a Gaussian filter ($\sigma = 1.5$) and the difference was normalized and used as an alpha channel in the final visualization. The alpha channel controls the saturation of each pixel in the final visualization, meaning an opaque color shows high certainty and a desaturated color shows low certainty.

Results and discussion

Locking point for drying maltodextrin droplets

Upon transformation into a dry particle, evolving temperature, moisture gradients and changing rheological behavior affect the drying, and so morphological and sticking behavior of drying droplets. After a short initial period of constant rate drying and isotropic shrinkage of the droplet, a concentration gradient develops, with the highest concentration of solutes close to the surface. For maltodextrin solutions, a sharp concentration gradient results in the formation of a viscoelastic skin, which initiates morphology development and is also relevant for predicting sticky behavior.[8] From the definition of the locking point, the locking point time is here determined from the point in time at which the ideally shrinking droplet becomes non-spherical, as determined by visual inspection. The locking point time was visually observed to be 6.5 ± 0.3 s.

The effect of varying glass bead size on collision outcomes

A complete overview of the collision outcomes for all time points, for each size range can be found in Figure 4. The collision outcomes are presented against the time of collision and the locking point is given, both as single datapoints and as distribution across each size range. The total number of collisions observed for each size range can be found in Table 1.

As expected, merging mostly occurs in the beginning of the drying as there is no skin formation yet. Especially before the locking point time (or $t_{collision}/t_{lock}<1$), merging is prevalent. It was hypothesized that a larger glass bead size would result in a later onset of the sticking and bouncing regime given the larger impulse of the glass bead and so larger surface deformation at the point of impact.[30] The obtained results did not confirm this, as can be seen in Figure 4, the onset of sticking and bouncing is approximately the same for all size ranges. The larger deformation of the skin caused by glass beads was confirmed by performing collisions between particles and wet droplets, so for our case it can be concluded the impact of drying and so the state of the droplet is more important in determining the collision outcomes. Similarly, van Boven et al.[21] concluded that differences in onset of stickiness regime were mainly due to droplet composition, which is similar for all experiments in this research. Outliers to this observation could possibly be explained by irregularities in skin formation if drying droplets are compared. A slightly higher temperature or smaller droplet could have an effect to some extent.

The collision outcomes observed are partially distributed, which may be explained by, for example, the particle size distribution within each category. Using kernel density estimation, probability plots were created to illustrate the likelihood of a particular collision outcome at a certain point in time. This can be a valuable addition to the dataset, especially for time points with no experimental observation of collisions. From Figure 5, it can be concluded that the probability of observing sticking differs for collisions between maltodextrin droplets and glass beads differing in size. For the largest three glass bead sizes, a longer stickiness regime is observed upon increasing glass bead size (Figure 4), especially later in time the probability of a collision resulting in sticking is high for larger glass beads (Figure 5). The increase is mostly at the

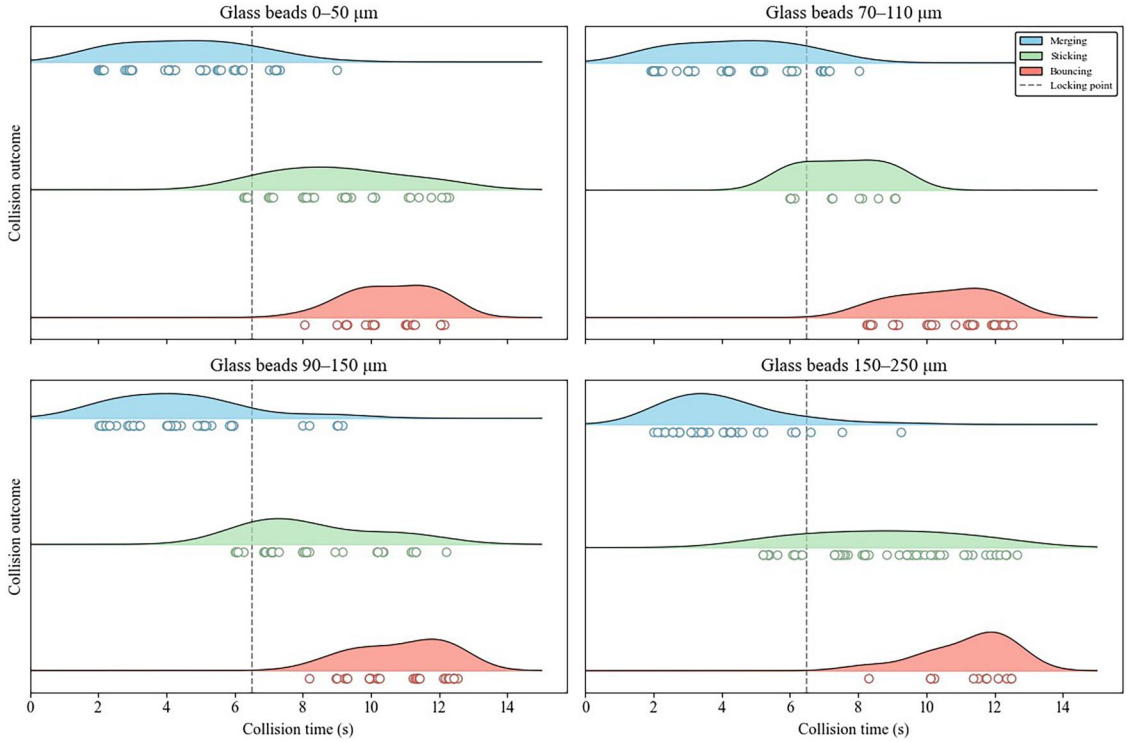

Figure 4. Collision outcomes over time for glass bead size ranges 0–50, 70–110, 90–150 and 150–250 µm, for merging (●), sticking (●), and bouncing (●); the dashed line indicates the locking point time.

Table 1. Overview of total number of collisions observed, for every size range.

Glass bead size range	Number of total collisions
0–50 µm	117
70–110 µm	128
90–150 µm	116
150–250 µm	109

cost of fewer bouncing collisions and was again expected to be caused by the larger impulse leading to easier penetration of the droplet surface, i.e. being able to break through the skin. Assuming the acceleration of the glass beads is similar for the different glass bead size ranges, the impulse of the collision is dominated by the mass. Given the glass beads are almost perfectly spherical, the mass of the bead is proportional to the cube of the radius (r^3). For that reason, as glass bead size increases the impulse exerted on the droplet becomes considerably larger. This in turn leads to more sticking collisions at later collision times.

In contrast to larger particles, the longer stickiness regime of the smallest glass beads can be explained by an increased relative contribution of colloidal forces, in the form of intermolecular van der Waals forces.[31] With an average particle size of 28 ± 0.5 µm colloidal forces become more significant compared to gravitational or inertial forces involved in the collision. Although the particle size exceeds the characteristic 10 µm threshold at which colloidal forces become comparable to or greater than gravitational forces, van der Waals forces cannot be ruled out. For example, for pharmaceutical powders it was found van der Waals forces play a large role when powder particles show poor flowability. Although smaller, this effect was also found for particles of 20–30 µm.[32,33] Besides, similar observations were found for collisions of particles with a wall, where the initial kinetic energy is insufficient to overcome the energy loss due to viscoelasticity and adhesion, leading to sticking of a particle.[34]

The current experimental approach provides first insights into droplet-fine collisions at small scale, however only for a single model material of the drying droplet. The obtained insights for glass beads of varying size range might differ if the droplet formulation would be different. It is, for example, expected that the effect of the inertial forces of the larger glass beads is smaller if maltodextrins with lower DE values are used for the drying droplet. Maltodextrins with lower DE values develop a more smooth and elastic skin upon drying.[11] Deformation of this skin due to drying is not possible on the time scale of the drying process, which ensures the skin is more stable against developed surface stresses.[35] For that reason, it could be of interest to extend the obtained findings for multiple formulations of the drying droplet. Similarly, it

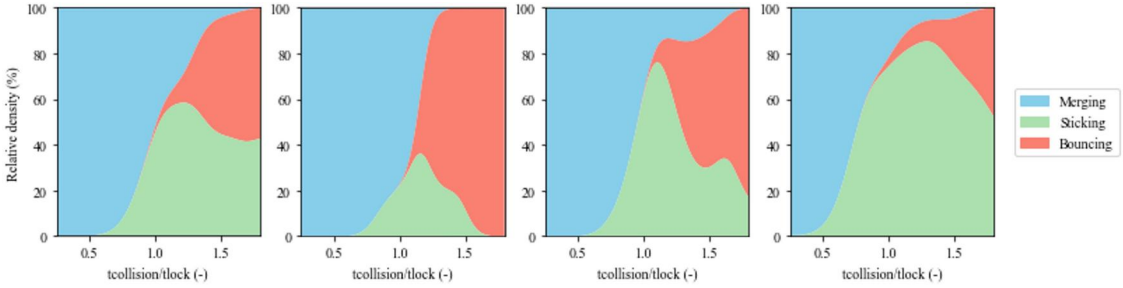

Figure 5. Stacked area charts for collisions between maltodextrin (DE38) droplets and glass beads differing in size, based on kernel density estimation values relative for each collision outcome for values of $t_{collision}/t_{lock}$ (-); again for merging (●), sticking (●), and bouncing (●).

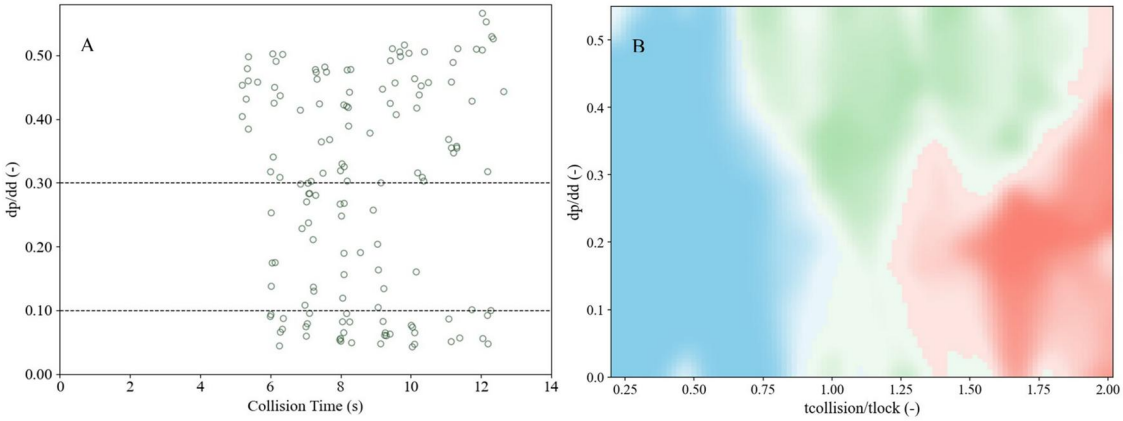

Figure 6. (A) Scatter plot of sticking collisions with d_p/d_d as a function of $t_{collision}/t_{lock}$. (B) Dominant outcome map for all collision outcomes with d_p/d_d as a function of $t_{collision}/t_{lock}$.

could be of interest to study the effect of drying conditions on skin formation, especially on skin thickness, and its effect on the stickiness regime.

Size-dependent trends beyond categorization

The four different size ranges described above were determined based on glass bead specifications provided by the supplier and so far, the results were therefore divided into these pre-distinguished size ranges as well. Rather than dividing the dataset into discrete size categories, the dataset is plotted into one figure using individual particle sizes. As explained in Section *Collision analysis* the true diameter of each glass bead was determined. When comparing the PSD_Matlab to the PSD_Mastersizer, minor differences are observed. Due to fewer data points, Figure A2 displays sharper transitions and reduced smoothness. Altogether, it was concluded that the particle diameter was determined accurately.

Given the stickiness regime is of most interest, a scatter plot was generated for a normalized particle diameter (particle diameter (d_p) over the droplet diameter (d_d)) against the normalized collision time. For all particle sizes, the stickiness regime commences around the same time. However, for $d_p/d_d < 0.1$ and $d_p/d_d > 0.3$ the stickiness regime clearly lasts longer, so the scatter plot (Figure 6(A)) could be divided into three parts as highlighted with a dashed line. This corresponds to a particle diameter smaller than 40 µm and larger than 120 µm, respectively, suggesting that categorization of the data according to these boundaries could improve the visualization of the collision data.

Moving beyond size-based categories, the dominant collision outcome and its spatial prevalence could be identified (Figure 6(B)). The separate probability fields constructed for each outcome emphasize regions where either one of the outcomes is most likely to occur. These figures are stacked to form the dominant outcome map, where each layer represented the interpolated likelihood of a specific outcome (merging, sticking or bouncing). A less saturated color indicates a higher uncertainty of a collision outcome being the dominant outcome. The transition from merging to sticking and sticking to bouncing is therefore least

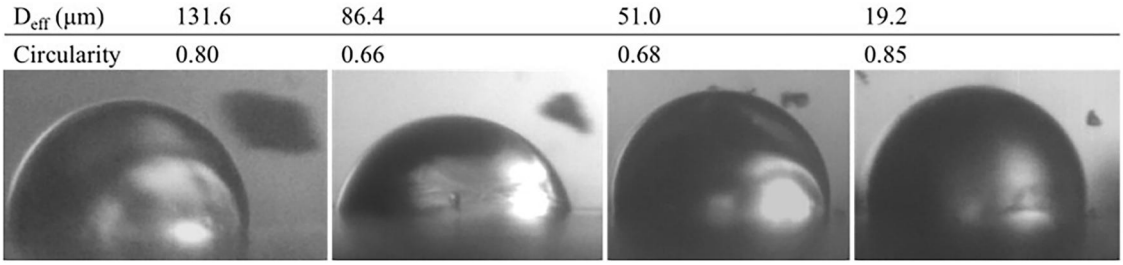

Figure 7. Overview of maltodextrin particles with different shapes and sizes colliding with drying maltodextrin droplets, the effective diameter of the maltodextrin particles is denoted by D_{eff}. The actual drying time differs for each snapshot, hence the drying droplets do not have a similar size.

saturated, as multiple outcomes have a high chance of occurring. Regardless of the normalized particle diameter a shift from merging to sticking to bouncing is observed, highlighting the dominant effect of the drying droplet on collision outcomes. Comparing Figures 5 and 6(B), especially the longer stickiness regime for larger particles is more pronounced in Figure 6(B), albeit with relatively high uncertainty. For moderate particle size of d_p/d_d of 0.1–0.3 the stickiness regime is shortest. For small particles the stickiness regime is a bit longer, with a somewhat higher uncertainty. Toward later collision times the bouncing regime becomes more prevalent for all size ranges. From the obtained results for varying glass bead sizes, whether the results are categorized or not, it can be concluded that larger glass beads lead to more sticking results. However, it can be questioned whether the largest size range accurately mimics collisions of fines, given both their size and their larger mass. For that reason, it is advised to carefully select a specific size range for binary collision experiments that mimic droplet-fine collisions.

Comparing collision material – the effect on collision outcome

Collisions between a drying droplet and dry particle are expected to be affected by the powder properties, such as size and shape, of the dry particle too. From literature it becomes clear that for example particle size and density affect agglomeration in fluid bed dryers and non-sphericity of particles affects collisions between particles and a wall in gas-solid flow.[36,37] The results presented earlier in this research show the effect of fines particle size on collision outcomes, and particularly the stickiness regime. The characteristics of glass beads do not exactly match those of fines, since glass beads are almost perfectly spherical and high in density. To examine whether non-spherical particles, lower in density affect collision outcomes, and to verify whether glass beads sufficiently mimic fines particles; maltodextrin powder particles were used as collision material. The size and shape of the maltodextrin DE 21 particles differs from particle to particle. As stated, the particle size distribution of maltodextrin powder roughly varies from 10 to 350 µm, where the shape of two similar sized particles could be quite different. A representative example of differences in shape and size of the particles can be found below, in Figure 7.

To study whether size and shape affect collision outcomes, similar collision experiments were carried out using the maltodextrin powder. An overview of the collision outcomes for all time points is presented below (Figure 8). Similar to the results using glass beads, the collision outcomes are presented against the time of collision, and a stacked area chart based on kernel density estimation is provided. Given the composition of the drying droplet and drying conditions were not altered, the locking point time is still 6.5 (± 0.3) seconds. In total 129 collisions were observed for collision times ranging from 1 to 11 s.

As expected, merging mostly occurs at the beginning of drying, roughly up until $t_{collision}/t_{lock}$ is 1. The merging regime is shorter when compared to collisions with glass beads. The higher mass of glass beads could have caused larger deformation, thereby ensuring total submerging of the glass beads when $t_{collision}/t_{lock} > 1$. In comparison, smaller spherical particles with similar velocities but greater size and mass it was found the deformation upon collision was much stronger.[38] In general, overlap between all 3 regimes is observed before the locking point time. The bouncing regime commences somewhat earlier on in the drying process, as in comparison, bouncing collisions occur roughly only from $t_{collision}/t_{lock}$ is >1 for glass beads. The early bouncing collisions could be due to the lower mass of maltodextrin fines, which leads to a smaller impulse imparted on the drying droplet upon collision. Regarding the stickiness regime, the earlier onset is striking. The extended stickiness regime for larger glass beads could be explained by the larger

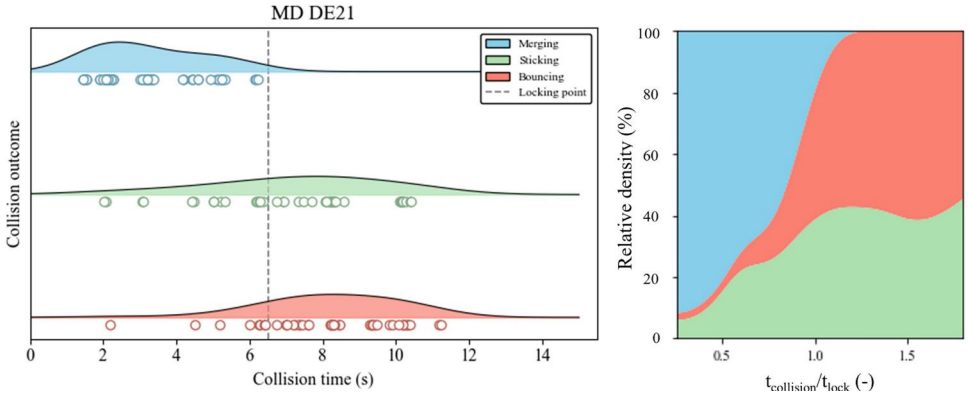

Figure 8. Collision outcomes over time for maltodextrin (DE21) particles, for merging (●), sticking (●), and bouncing (●), the dashed line indicates the locking point time; and stacked area chart, based on kernel density estimation values relative for each collision outcome for values of $t_{collision}/t_{lock}$ (-); merging (●), sticking (●), and bouncing (●).

inertial forces exerted on the droplet. In contrast, the lower mass and irregular shape of the particles could increase the surface contact area between the drying droplet and dry particle upon collision, thereby increasing the chance of sticking. However, the fact that no categorization was applied was considered the main reason for the longer stickiness regime. The size distribution of the MD particles covers the size range of all four glass bead size ranges, put together in one figure, so the size variations of the colliding particles most probably explain the extended stickiness regime. This effect is especially visible in the stacked area chart, where the chance of a collision resulting in sticking does not seem to decrease much after $t_{collision}/t_{lock} = 1.5$. Unfortunately, due to the limited number of data points, the collisions of the maltodextrin particles could not be categorized in the same manner as those of the glass beads. This limitation increases the complexity of achieving a fair comparison between the results of the two colliding particle types. For extending this research in the future, it would be useful to utilize similar size categories for easier direct comparison of multiple dry particle types. Still, a comparison between glass beads and maltodextrin particles does not reveal any large differences, given merging, sticking and bouncing occur sequentially and sticking is most pronounced around the locking point time. As no fundamentally different conclusions are drawn, glass beads seem to be adequately mimicking droplet-fine collisions occurring in spray dryers, provided that careful size-selection is performed.

The effect of maltodextrin shape and size on the stickiness regime

The differences between glass beads and maltodextrin particles were further studied through image analysis. For colliding maltodextrin particles that resulted in a sticking collision the particle effective diameter and circularity were determined, this concerned 36 collisions. The particle area (A) was calculated by determining all pixels within the boundary. For direct comparison to glass beads, an effective diameter (D_{eff}) was determined from the particle area. A spherical geometry was assumed for the calculation, and D_{eff} was determined using equation 1:

$$A = {D_{eff}}^2 * \frac{\pi}{4} \tag{1}$$

For 2D images, the shape descriptor circularity provides a measure of how closely an object's shape approximates that of a perfect circle, it can be determined using different formulae.[39] For this research the formula proposed by Wadell[40] was used, which describes the ratio of the perimeter (P) of a circle with the same area as the object to the actual perimeter of the object, and is calculated as follows:

$$Circularity = \frac{2\sqrt{\pi A}}{P} \tag{2}$$

A value between 0 and 1 is computed, where a larger deviation from 1 describes a particle that is more elongated, irregular, or jagged. Both circularity and D_{eff} of the maltodextrin particles as a function of collision time can be found in Figure 9.

Inspection of the figure above reveals that generally maltodextrin particles do not greatly differ from a spherical shape, with the largest deviation and so the lowest circularity value being 0.60 and the highest value being 1. It was found that around 70% of the particles have a circularity value of 0.8 or higher. Also, it was previously found for drying maltodextrin droplets that the sticky region ranges from approximately 0.75 to 1.5 times the locking point time.[20] Within this highlighted region the full variation of

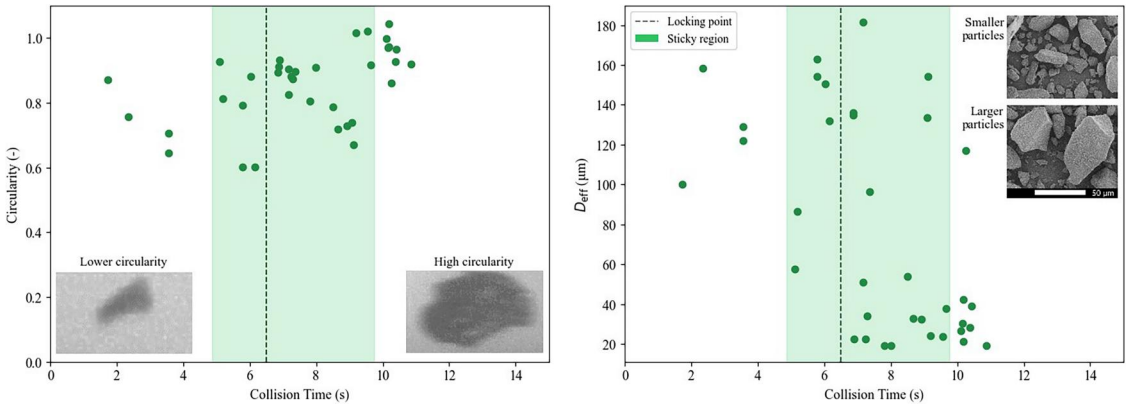

Figure 9. Particle circularity (left) and effective diameter (D_{eff}) (right) of the maltodextrin powder particles that resulted in a sticking collision, as a function of collision time. The locking point is given and the sticky region is highlighted.

circularities of MD particles is observed. So, it can be concluded that the state of the droplet is more dominant in determining the collision outcome than the particle shape of the colliding dry particle.

For sticking collisions, almost the same range of particles sizes was observed, if compared to glass beads as revealed by the effective diameter, only the largest sizes do not appear in the dataset. It can be observed in Figure 9 that, irrespective of the particle size, most particles stick within the highlighted sticky region. Again, it can be concluded here the drying droplet has a larger effect on a collision resulting in sticking, than the size of the dry maltodextrin particle. This conclusion counteracts the findings of a previous section, given glass bead size did affect collision outcomes to some extent. The biggest difference between the dry particles is the density and so mass, and the increased impulse upon collision for large glass beads. For that reason, it is advised to carefully select a glass bead size range when mimicking droplet-fine collisions. Lastly, at later collision times, smaller particles seem to also stick to the drying droplet, which is expected to be caused by colloidal forces such as van der Waals interactions or hydrogen bonding. These findings resemble the findings of the smallest glass bead size range.

Conclusions

With this study, it was aimed to gain insights into collisions of fines particles and droplets for drying conditions relevant to nozzle zone agglomeration in spray drying. Specifically, the effect of particle size and shape on binary collisions between drying droplets and dry particles were studied. Using a single droplet drying approach, maltodextrin droplets were dried and collisions with dry particles were observed at different time points during drying. The effect of size was tested using four different size ranges of glass beads. Given in real spray drying processes fines particles do not have such a high density as glass beads and are irregularly shaped, maltodextrin powder was also used as collision material.

For glass beads, upon drying collisions first resulted in merging, followed by sticking and bouncing, with sticking being most pronounced around the locking point time. For the largest three size ranges, more sticking collisions occurred, mainly at the cost of bouncing collisions, upon increasing glass bead size range. This was attributed to the higher mass and impulse of larger glass beads. Without categorizing the data, the longer stickiness regime observed for collisions with larger particles was more pronounced. No vastly different conclusions were drawn, other than the size of the particle to mimic fines should be chosen carefully, which could potentially be identified using this mapping approach.

For collisions with maltodextrin particles, the stickiness regime commenced somewhat earlier and lasted longer, mainly because data were not categorized into size ranges. If glass beads and maltodextrin are compared, the high mass of glass beads led to complete submerging of the glass bead at later drying times and the maltodextrin particle properties caused earlier sticking collisions. However, the differences were minor, so it could be concluded that glass beads suffice for mimicking collisions with fines particles, although a representative glass bead size needs to be selected. Lastly, the shape of maltodextrin particles does not greatly differ from a spherical shape. Also, irrespective of shape and size of the maltodextrin particles, most sticking collisions were observed within the previously established sticky region. From that it

was concluded the state of the drying droplet is more dominant in determining collision outcomes.

Collision studies could be extended by studying different formulations of the drying droplet or using different drying conditions. The currently obtained insights provide new information on the sticking of particles upon collisions. The data could be useful input for model development, which could aid in predicting the stickiness regimes of drying droplets. This is necessary for establishing guidelines for nozzle zone agglomeration in spray drying.

Acknowledgements

Partners in this project are, Danone, dsm-firmenich, FrieslandCampina, Wageningen University & Research. Technical University of Eindhoven (TU/e) and ISPT. This project is co-funded with subsidy from the Topsector Energy by the Dutch Ministry of Economic Affairs and Climate Policy. More information can be found at https://ispt.eu/projects/dragonsegg/. We would like to thank the people from Technical Development Studio of Wageningen University & Research, for developing the single droplet dryer.

Disclosure statement

The authors declare that they have no known competing financial interests or personal relationships that could have appeared to influence the work reported in this paper.

Funding

This work is an Institute for Sustainable Process Technology (ISPT) project, i.e. Dragons Egg (Project number: DR-50-20).

Data availability statement

Data will be made available on request.

References

[1] Gianfrancesco, A.; Turchiuli, C.; Dumoulin, E. Powder Agglomeration during the Spray-Drying Process: Measurements of Air Properties. *Dairy Sci. Technol.* **2008**, *88*, 53–64. DOI: 10.1051/dst:2007008.

[2] Verdurmen, R. E. M.; Menn, P.; Ritzert, J.; Blei, S.; Nhumaio, G. C. S.; Sonne Sørensen, T.; Gunsing, M.; Straatsma, J.; Verschueren, M.; Sibeijn, M.; et al. Simulation of Agglomeration in Spray Drying Installations: The EDECAD Project. *Drying Technol.* **2004**, *22*, 1403–1461. DOI: 10.1081/DRT-120038735.

[3] Williams, A. M.; Jones, J. R.; Paterson, A. H. J.; Pearce, D. L. Effect of Fines on Agglomeration in Spray Dryers: An Experimental Study. *Int. J. Food Eng.* **2009**, *5*, DOI: 10.2202/1556-3758.1635.

[4] Turchiuli, C.; Gianfrancesco, A.; Palzer, S.; Dumoulin, E. Evolution of Particle Properties during Spray Drying in Relation with Stickiness and Agglomeration Control. *Powder Technol.* **2011**, *208*, 433–440. DOI: 10.1016/j.powtec.2010.08.040.

[5] van Boven, A. P.; Calderon Novoa, S. M.; Kohlus, R.; Schutyser, M. A. I. Investigation on Nozzle Zone Agglomeration during Spray Drying Using Response Surface Methodology. *Powder Technol.* **2023**, *429*, 118910. DOI: 10.1016/j.powtec.2023.118910.

[6] Roos, Y.; Karel, M. Phase Transitions of Mixtures of Amorphous Polysaccharides and Sugars. *Biotechnol. Prog.* **1991**, *7*, 49–53. DOI: 10.1021/bp00007a008.

[7] Truong, V.; Bhandari, B. R.; Howes, T. Optimization of Cocurrent Spray Drying Process for Sugar-Rich Foods. Part II—Optimization of Spray Drying Process Based on Glass Transition Concept. *J. Food Eng.* **2005**, *71*, 66–72. DOI: 10.1016/j.jfoodeng.2004.10.018.

[8] Both, E. M.; Karlina, A. M.; Boom, R. M.; Schutyser, M. A. I. Morphology Development during Sessile Single Droplet Drying of Mixed Maltodextrin and Whey Protein Solutions. *Food Hydrocoll.* **2018**, *75*, 202–210. DOI: 10.1016/j.foodhyd.2017.08.022.

[9] Tran, T. T. H.; Avila-Acevedo, J. G.; Tsotsas, E. Enhanced Methods for Experimental Investigation of Single Droplet Drying Kinetics and Application to Lactose/Water. *Dry. Technol.* **2016**, *34*, 1185–1195. DOI: 10.1080/07373937.2015.1100202.

[10] Li, B.; Jia, F.; Cao, Y.-P.; Feng, X.-Q.; Gao, H. Surface Wrinkling Patterns on a Core-Shell Soft Sphere. *Phys. Rev. Lett.* **2011**, *106*, 234301. DOI: 10.1103/PhysRevLett.106.234301.

[11] Siemons, I.; Politiek, R. G. A.; Boom, R. M.; van der Sman, R. G. M.; Schutyser, M. A. I. Dextrose Equivalence of Maltodextrins Determines Particle Morphology Development during Single Sessile Droplet Drying. *Food Res. Int.* **2020**, *131*, 108988. DOI: 10.1016/J.FOODRES.2020.108988.

[12] Sadek, C.; Schuck, P.; Fallourd, Y.; Pradeau, N.; Le Floch-Fouéré, C.; Jeantet, R.; Sadek, C.; Fallourd, Y.; Pradeau, N.; Schuck, P.; et al. Drying of a Single Droplet to Investigate Process–Structure–Function Relationships: A Review. *Dairy Sci. Technol.* **2015**, *95*, 771–794. DOI: 10.1007/s13594-014-0186-1.

[13] Sadek, C.; Pauchard, L.; Schuck, P.; Fallourd, Y.; Pradeau, N.; Le Floch-Fouéré, C.; Jeantet, R. Mechanical Properties of Milk Protein Skin Layers after Drying: Understanding the Mechanisms of Particle Formation from Whey Protein Isolate and Native Phosphocaseinate. *Food Hydrocoll.* **2015**, *48*, 8–16. DOI: 10.1016/j.foodhyd.2015.01.014.

[14] Eijkelboom, N. M.; van Boven, A. P.; Siemons, I.; Wilms, P. F. C.; Boom, R. M.; Kohlus, R.; Schutyser, M. A. I. Particle Structure Development during Spray Drying from a Single Droplet to Pilot-Scale Perspective. *J. Food Eng.* **2023**, *337*, 111222. DOI: 10.1016/j.jfoodeng.2022.111222.

[15] Both, E. M.; Boom, R. M.; Schutyser, M. A. I. Particle Morphology and Powder Properties during Spray Drying of Maltodextrin and Whey Protein Mixtures. *Powder Technol.* **2020**, *363*, 519–524. DOI: 10.1016/j.powtec.2020.01.001.

[16] Schutyser, M. A. I.; Perdana, J.; Boom, R. M. Single Droplet Drying for Optimal Spray Drying of Enzymes and Probiotics. *Trends Food Sci. Technol.* **2012**, *27*, 73–82. DOI: 10.1016/j.tifs.2012.05.006.

[17] Schutyser, M. A. I.; Both, E. M.; Siemons, I.; Vaessen, E. M. J.; Zhang, L. Gaining Insight on Spray Drying Behavior of Foods via Single Droplet Drying Analyses. *Dry. Technol.* **2019**, *37*, 525–534. DOI: 10.1080/07373937.2018.1482908.

[18] Sewalt, E. J. G. Predicting Collision Outcomes of Partially-Dried Droplets in Spray Drying. **2024**. DOI: 10.4233/uuid:8204cf4d-a5fd-4e20-956c-37aba9bf3dd7.

[19] Al-Khattawi, A.; Bayly, A.; Phillips, A.; Wilson, D. The Design and Scale-up of Spray Dried Particle Delivery Systems. *Expert Opin. Drug Deliv.* **2018**, *15*, 47–63. DOI: 10.1080/17425247.2017.1321634.

[20] Eijkelboom, N. M.; Rang, V. J.; Breevaart, S.; Boom, R. M.; Wilms, P. F. C.; Schutyser, M. A. I. Binary Collisions of Drying Maltodextrin Droplets and Glass Beads. *J. Food Eng.* **2024**, *378*, 112110. DOI: 10.1016/j.jfoodeng.2024.112110.

[21] van Boven, A. P.; Eijkelboom, N. M.; Fentsahm, K. J.; Gruson, M. J.; Boom, R. M.; Wilms, P. F. C.; Kohlus, R.; Schutyser, M. A. I. A Multiscale Investigation on Protein Addition toward Steering Agglomeration and Yield in Spray Drying. *LWT* **2024**, *212*, 116998. DOI: 10.1016/j.lwt.2024.116998.

[22] Selvamuthukumaran, M.; Tranchant, C.; Shi, J. Spray Drying - Concept, Application and Its Recent Advances in Food Processing. In *Handbook on Spray Drying Applications for Food Industries*; Selvamuthukumaran, M., Ed.; CRC Press - Taylor & Francis Group, **2019**.

[23] Vijaya Madhavi, V.; Kumari, P. L. S. A Qualitative Approach for Enhancing Fundus Images with Novel CLAHE Methods. *Eng. Technol. Appl. Sci. Res.* **2025**, *15*, 20102–20107. DOI: 10.48084/etasr.9525.

[24] Ge, M.; Hong, Q.; Zhang, L. **2018** A Hybrid DCT-CLAHE Approach for Brightness Enhancement of Uneven-Illumination Underwater Images. *ACM.* International Conference Proceeding Series, 123–127. DOI: 10.1145/3301506.3301539.

[25] Mohd Noor, M. H.; Hussain, Z.; Ahmad, K. A.; Ainihayati, A. R. **2011** Gel Electrophoresis Image Segmentation with Otsu Method Based on Particle Swarm Optimization. Proceedings - 2011 IEEE 7th International Colloquium on Signal Processing and Its Applications, CSPA 2011, 426–429. DOI: 10.1109/CSPA.2011.5759915.

[26] Sindhuri, M. S.; Anusha, N. **2016** Text Separation in Document Images through Otsu's Method. Proceedings of the 2016 IEEE International Conference on Wireless Communications, Signal Processing and Networking, WiSPNET 2016, 2395–2399. DOI: 10.1109/WiSPNET.2016.7566571.

[27] Ananthanarasimhan, J.; Leelesh, P.; Anand, M. S.; Lakshminarayana, R. Validation of Projected Length of the Rotating Gliding Arc Plasma Using "Regionprops" Function. *Plasma Res. Express* **2020**, *2*, 035008. DOI: 10.1088/2516-1067/abae49.

[28] Faruq, A.; Abdullah, S. S.; Marto, A.; Bakar, M. A. A.; Hussein, S. F. M.; Razali, C. M. C. The Use of Radial Basis Function and Non-Linear Autoregressive Exogenous Neural Networks to Forecast Multi-Step Ahead of Time Flood Water Level. *Int. J. Adv. Intell. Inform.* **2018**, *5*, 1–10. DOI: 10.26555/ijain.v5i1.280.

[29] Roshani, G. H.; Karami, A.; Salehizadeh, A.; Nazemi, E. The Capability of Radial Basis Function to Forecast the Volume Fractions of the Annular Three-Phase Flow of Gas-Oil-Water. *Appl. Radiat. Isot.* **2017**, *129*, 156–162. DOI: 10.1016/j.apradiso.2017.08.027.

[30] Gao, Y.; Mitra, S.; Wanless, E. J.; Moreno-Atanasio, R.; Evans, G. M. Interaction of a Spherical Particle with a Neutrally Buoyant Immiscible Droplet in Salt Solution. *Chem. Eng. Sci.* **2017**, *172*, 182–198. DOI: 10.1016/j.ces.2017.06.018.

[31] Li, S.; Marshall, J. S.; Liu, G.; Yao, Q. Adhesive Particulate Flow: The Discrete Element Method and Its Application in Energy and Environmental Engineering. *Prog. Energy Combus. Sci.* **2011**, *37*, 633–668. DOI: 10.1016/j.pecs.2011.02.001.

[32] Capece, M.; Silva, K. R.; Sunkara, D.; Strong, J.; Gao, P. On the Relationship of Inter-Particle Cohesiveness and Bulk Powder Behavior: Flowability of Pharmaceutical Powders. *Int. J. Pharm.* **2016**, *511*, 178–189. DOI: 10.1016/J.IJPHARM.2016.06.059.

[33] Li, Q.; Rudolph, V.; Weigl, B.; Earl, A. Interparticle van Der Waals Force in Powder Flowability and Compactibility. *Int. J. Pharm.* **2004**, *280*, 77–93. DOI: 10.1016/J.IJPHARM.2004.05.001.

[34] Zhang, Y.; Fang, Z.; Zhao, S.; Wei, M.; Wu, X.; Sun, L. An Experimental Study on the Wall Collision of Micro-Sized Graphite Particles by High-Speed Photomicrography. *Prog. Nucl. Energy* **2020**, *125*, 103391. DOI: 10.1016/j.pnucene.2020.103391.

[35] Siemons, I.; Veser, J.; Boom, R. M.; Schutyser, M. A. I.; van der Sman, R. G. M. Rheological Behaviour of Concentrated Maltodextrins Describes Skin Formation and Morphology Development during Droplet Drying. *Food Hydrocoll.* **2022**, *126*, 107442. DOI: 10.1016/j.foodhyd.2021.107442.

[36] Cen, Z.; Wu, Y.; Wang, J.; Liu, J.; Zhou, M.; Chen, S.; Zhao, D. Investigation of the Dominant Effects of Non-Spherical Particles on Particle–Wall Collisions. *Processes* **2024**, *12*, 1234. DOI: 10.3390/pr12061234.

[37] Shabanian, J.; Duchesne, M. A.; Syamlal, M.; Runstedtler, A. A Generalized Analytical Energy Balance Model for Evaluating Agglomeration from a Binary Collision of Wet Particles. *Heliyon* **2024**, *10*, e26320. DOI: 10.1016/J.HELIYON.2024.E26320.

[38] Sommerfeld, M.; Huber, N. Experimental Analysis and Modelling of Particle-Wall Collisions. *Int. J. Multiphase Flow* **1999**, *25*, 1457–1489. DOI: 10.1016/S0301-9322(99)00047-6.

[39] Blott, S. J.; Pye, K. Particle Shape: A Review and New Methods of Characterization and Classification. *Sedimentology* **2008**, *55*, 31–63. DOI: 10.1111/j.1365-3091.2007.00892.x.

[40] Wadell, H. Sphericity and Roundness of Rock Particles. *J. Geol.* **1933**, *41*, 310–331. DOI: 10.1086/624040.

Appendix

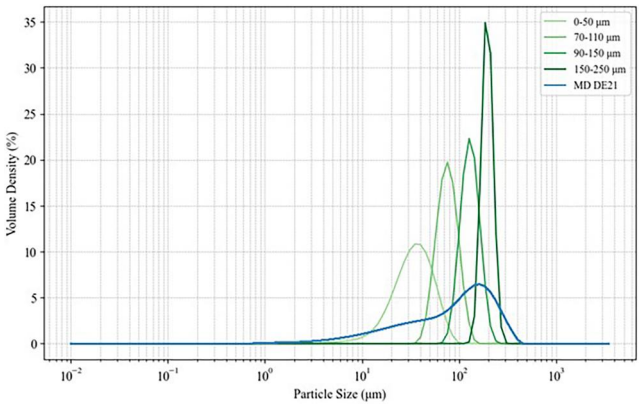

Figure A1. Particle size distribution of glass bead size ranges and MD powder mixed with flow aid Sipernat 380 (PSD_Mastersizer).

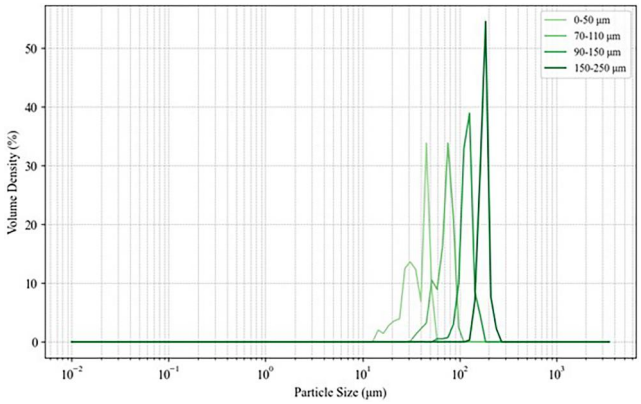

Figure A2. Particle size distribution of colliding glass beads, as determined using image analysis (PSD_Matlab).

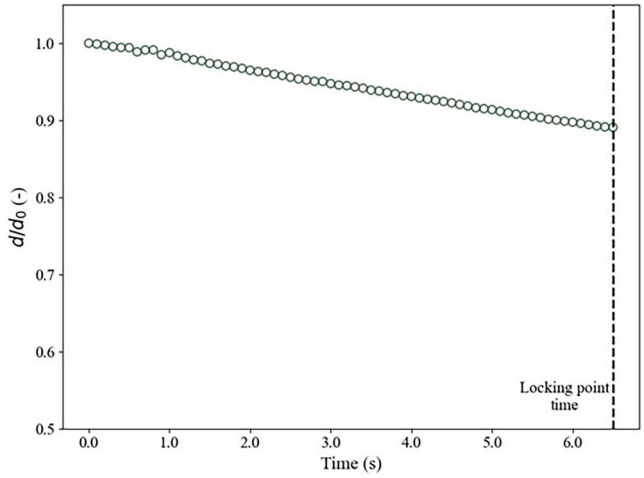

Figure A3. Average droplet diameter decrease due to evaporation, up until the locking point.

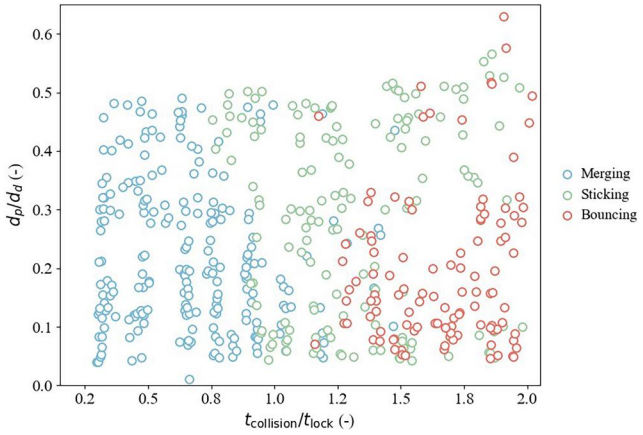

Figure A4. Complete dataset of normalized particle diameter over normalized collision time, for all collision outcomes.